Electronic Supplementary Material (ESI) for Chemical Communications.

Supporting Information

Semiconducting silicon-phosphorous frameworks for caging exotic polycations

Philip Yox,[a,b] Andrew P. Porter,[a] Rick W. Dorn,[a,b] Victoria Kyveryga,[a] Aaron J. Rossini,[a,b] Kirill Kovnir[a,b,*]

[a] *Department of Chemistry, Iowa State University, Ames, IA 50011, United States*

[b] *Ames Laboratory, U.S. Department of Energy, Ames, IA 50011, United States*

* Corresponding author: kovnir@iastate.edu

Experimental

Synthesis. Starting materials used were Ba dendrites (Sigma Aldrich, 99.9%), Sr dendrites (Sigma Aldrich 99.9%), Si powder (Alfa Aesar 99.99%), red P powder (Alfa Aesar 98.90%), NaCl (Sigma Aldrich 99%), KCl (Sigma Aldrich 99.5%), RbCl (Sigma Aldrich 99.8%), RbBr (Sigma Aldrich 99.7%), RbI (Sigma Aldrich 99.8%), CsCl (Sigma Aldrich 99.99%), CsBr (Alfa Aesar 99%), CsI (Alfa Aesar 99.9%). Materials were used as received and handled in an Ar filled glovebox with O_2 < 0.1 ppm. Materials were loaded into carbonized, fused silica tubes, evacuated and flame-sealed.
Stoichiometric Synthesis: The alkali metal salt, alkaline-earth metal (Ba/Sr), silicon, and phosphorus, were loaded in their stoichiometric ratios (1:6:12:20) with a total mass of 0.25 g into carbonized, fused silica ampoules. Samples were then heated (see Table S1) and either slow cooled or annealed. The samples were ground finely in the glovebox, resealed, and heated again.
Synthesis From Salt-Flux: The alkaline-earth metal, silicon, and phosphorus were loaded in their stoichiometric ratios (6:12:20) with a total mass of 0.25 g into carbonized, fused silica ampoules. The alkali metal salt (0.25 g) was then loaded. The fused silica ampoules were sealed, then placed in the furnace for heating (see Table S1). After cooling, in some cases, mm-sized crystals were found deposited on the walls of ampoule above the solid salt indicating a transport reaction occurred. However, many crystals (often grown together see Figure S1) could also be found in the salt, suggesting nucleation and growth from the liquid.

Powder Xray Diffraction (PXRD). PXRD experiments were performed using a Rigaku Miniflex 600 (Cu-K_α radiation with Ni-K_β filter). Data was collected with a 0.02° step at 10° per minute.

Single Crystal Xray Diffraction. Single crystal Xray diffraction was performed on a Bruker D8 Venture diffractometer (Mo-K_α radiation). Data was collected at 100 K with φ and ω scans recorded at a 0.3° step and integrated using the Bruker SAINT software package. Multi scan absorption correction was used. Structure solution and subsequent refinement was carried out

with the SHELX suite.[1] The initial structure solution was obtained via intrinsic methods. The atom type assignment was refined based on the peak/hole optimization, atomic displacement parameters, and chemical environment/coordination. While Si and P have similar scattering factors, P should be closer to the cations as well as capable of three and two coordinate configurations. In materials containing Cs and Ba, the difference in scattering factor was not large enough to reliably refine joint occupancy. Due to the distance between cation and P, the larger cation, Cs, was chosen to reside at the 4*b* site exclusively. For other materials not containing both Cs and Ba, the occupancies of the 24*e* and 4*b* sites were refined jointly with both the alkali metal and alkaline earth metal. Constraints were applied to the displacement parameters so that jointly occupied atoms had the same displacement parameters. The total occupancy of each site was constrained to be 100%. The total number of alkali metal atoms and alkali-earth metals were also constrained to be 4 and 24, respectively. In some cases, the 4*b* site was split into another 24*e* site (see Table S4) and constraints were managed in a similar manner. For Br- and Cl-containing compounds, the halogen site shows no deviation from 100% occupancy. In turn, the compounds containing iodine had a large negative peak at the iodine position. Upon refining the occupancy of the site, the iodine position seemed to contain vacancies (see Table S4). Upon reevaluating the occupation of the cation positions in these cases, removing the constraints on the ratio of alkali metal to alkaline-earth metal resulted in a composition that would be charge balanced, *e.g.* $RbBa_6Si_{12}P_{20}I_{0.9}$ was further refined to be $Rb_{1.1}Ba_{5.9}Si_{12}P_{20}I_{0.9}$.

Differential Scanning Calorimetry (DSC). Calorimetry experiments were performed with a Netzsch DSC 404 F3 Pegasus. Approximately 25 mg of $CsBa_6Si_{12}P_{20}Br$ was sealed in an evacuated silica ampoule and measured against a nearly identical but empty silica ampoule. Calorimetry measurements were taken from 200°C to 1100°C.

Diffuse Reflectance Spectroscopy. A BLACK-Comet C-SR-100 spectrometer was used to measure the UV/vis diffuse reflectance spectra from 200 to 1080 nm. Band gaps were estimated through extrapolation of the linear slope in the Tauc plots by plotting $(Ahv)^{1/r}$ vs hv where r = ½ for direct and r = 2 for indirect band gaps.

Computational Methods. Band structure, density of states, and electron localization function (ELF) were calculated with the tight-binding linear muffin-tin orbital atomic sphere approximation (TB-LMTO-ASA) package.[2] The program, ParaView, was used for visualization of ELF.[3]

Solid-State NMR Spectroscopy. All experimental solid-state NMR parameters (magnetic field strength (B_0), MAS frequency, recycle delay, number of scans, t_1 TD points, t_1 dwell (Δt_1) and total experimental times) are given in Table S6. $CsBa_6Si_{12}P_{20}Cl$ was packed into a 4 mm zirconia NMR rotor inside an Ar filled glovebox and spun with N_2 gas to avoid air/moisture exposure. ^{29}Si, ^{31}P, ^{35}Cl, and ^{133}Cs chemical shifts were indirectly referenced to ^{1}H chemical shifts of 1 % tetramethylsilane in $CDCl_3$ with adamantane as a secondary chemical shift reference ($\delta_{iso}(^1H)$ = 1.70 ppm) using the previously published IUPAC recommended relative NMR frequencies.[4] All NMR spectra were processed in Bruker Topspin 3.6.1. ^{29}Si, ^{31}P, and ^{133}Cs NMR spectra were analytically simulated using the solid lineshape analysis (sola) module as implemented in Bruker Topspin 3.6.1.

B_0 = 9.4 T. Solid-state NMR experiments were recorded on a 9.4 T ($\nu_0(^1H)$ = 400 MHz) Bruker wide-bore magnet equipped with a Bruker AVANCE III HD console and a 4.0 mm HXY magic-angle spinning (MAS) NMR probe. The probe was configured in HX double resonance

mode for all 1D ^{29}Si, ^{31}P, ^{35}Cl, and ^{133}Cs NMR experiments. To enable ^{31}P-^{133}Cs heteronuclear correlation NMR experiments, the probe was configured in triple-resonance HXY mode with a 1000 pF shunt capacitator placed in parallel with the Y-channel. The following radio frequency (RF) pulses correspond to the probe in HX double resonance mode. ^{31}P $\pi/2$ and π pulse lengths were 3.5 and 7 μs in duration, corresponding to an *ca.* 71 kHz RF field. ^{29}Si $\pi/2$ and π pulse lengths were 5 and 10 μs in duration, corresponding to a 50 kHz RF field. ^{35}Cl central-transition (CT) selective $\pi/2$ and π pulse lengths were 10 and 20 μs in duration, corresponding to a 12.5 kHz RF field and 25 kHz CT nutation frequency. ^{133}Cs $\pi/2$ and π pulse lengths were 8.75 and 17.5 μs in duration, corresponding to an *ca.* 29 kHz RF field. We note that the ^{133}Cs pulses were solution-like and not CT selective because of the small ^{133}Cs quadrupolar interaction. In triple-resonance ^{1}H-^{31}P-^{133}Cs mode, ^{31}P $\pi/2$ and π pulse lengths were 5.75 and 11.5 μs in duration, and the ^{133}Cs $\pi/2$ pulse length was 10 μs in duration. ^{31}P and ^{133}Cs longitudinal relaxation constants (T_1) were determined via a saturation recovery NMR experiment. ^{29}Si T_1 was estimated by recording multiple ^{29}Si spin echo NMR spectra with different recycle delays (Figure S6). 1D ^{31}P and ^{133}Cs NMR spectra were recorded with recycle delays ≥ 5 × T_1, while the 1D ^{29}Si NMR spectrum was recorded with a recycle delay ~ 3-4 × T_1. 2D ^{133}Cs chemical exchange (EXSY) spin-diffusion spectra were recorded with either 1 μs or 0.5 s of Z spin-diffusion and a sample temperature of *ca.* 38 or 58 °C. The temperature of the sample was determined by packing a small amount of KBr in the rotor and measuring the ^{79}Br T_1.[5] 2D ^{31}P{^{133}Cs} D-HMQC NMR experiments were performed with previously described pulse sequences.[6] 0.8 or 4.0 ms of 62.5 kHz RF field Rotation-Echo DOuble Resonance (REDOR) recoupling was applied to the ^{31}P spins to re-introduce the ^{31}P-^{133}Cs dipolar interaction under MAS.[7]

B_0 = 14.1 T. A 1D ^{133}Cs solid-state NMR spectrum was recorded on a 14.1 T (ν_0(^{1}H) = 600 MHz) Bruker wide-bore magnet spectrometer equipped with a Bruker AVANCE NEO console and a 4 mm HXY MAS probe configured in double-resonance mode. The 1D ^{133}Cs NMR spectrum was acquired with a 90° tip-angle single pulse NMR experiment. The ^{133}Cs $\pi/2$ pulse length was 10 μs in duration, corresponding to a 25 kHz RF field.

[1] Sheldrick, G. M. A Short History of SHELX. *Acta Crystallographica Section A* **2008**, 64 (1), 112-122. https://doi.org/10.1107/S0108767307043930.

[2] a) Jepsen, O.; Burkhardt, A.; Andersen, O.K. *The Program TB-LMTO-ASA. Version 4.7*. Max-Planck-Institut für Festkörperforschung, Stuttgart, 1999; b) A. D. Becke and K. E. Edgecombe, *J. Chem. Phys.,* 1990, **92**, 5397; c) A. Savin, O. Jepsen, J. Flad, O. K. Andersen, H. Preuss, and H. G. von Schnering, *Angew. Chem. Int. Ed. Engl.,* 1992, **31***,* 187-188; d) 26. A. Savin, R. Nesper, S. Wengert, and T. F. Fässler, *Angew. Chem. Int. Ed. Engl.* 1997, ***36****,* 1808-1832; e) Y. Grin, A. Savin, B. Silvi, in *The Chemical Bond: Fundamental Aspects of Chemical Bonding,* Eds.: G. Frenking, S. Shaik, Wiley-VCH, Weinheim, 2014**,** 10, 345-382.

[3] a) Sandia National Labs, Kitware Inc, Los Alamos National Labs, Paraview: Parallel visualization application, version 4.1.0 64-bit, USA, http://paraview.org; b) A.I. Baranov, *Visualization plugin for ParaView*. 2012.

[4] R. K. Harris, E. D. Becker, S. M. Cabral de Menezes, R. Goodfellow, P. Granger. *Solid State Nucl. Magn. Res.*. **2002**, *22*, 458-483.

[5] K. R. Thurber, R. Tycko, *J. Magn. Res.* **2009,** *196,* 84-87.

[6] a) J. Trebosc, B. Hu, J.P. Amoureux, Z. Gan, *J. Magn. Res.* **2007,** *186,* 220-227; b) I. Hung, A.-C. Uldry, J. Becker-Baldus, A.L. Webber, A. Wong, M. E. Smith, S. A. Joyce, J. R. Yates, C. J. Pickard, R. Dupree, S. P. Brown *J. Amer. Chem. Soc.* **2009** *131*, 1820-1834.

[7] T. Gullion, J. Schaefer, *J. Magn. Res.* **1989,** *81,* 196-200.

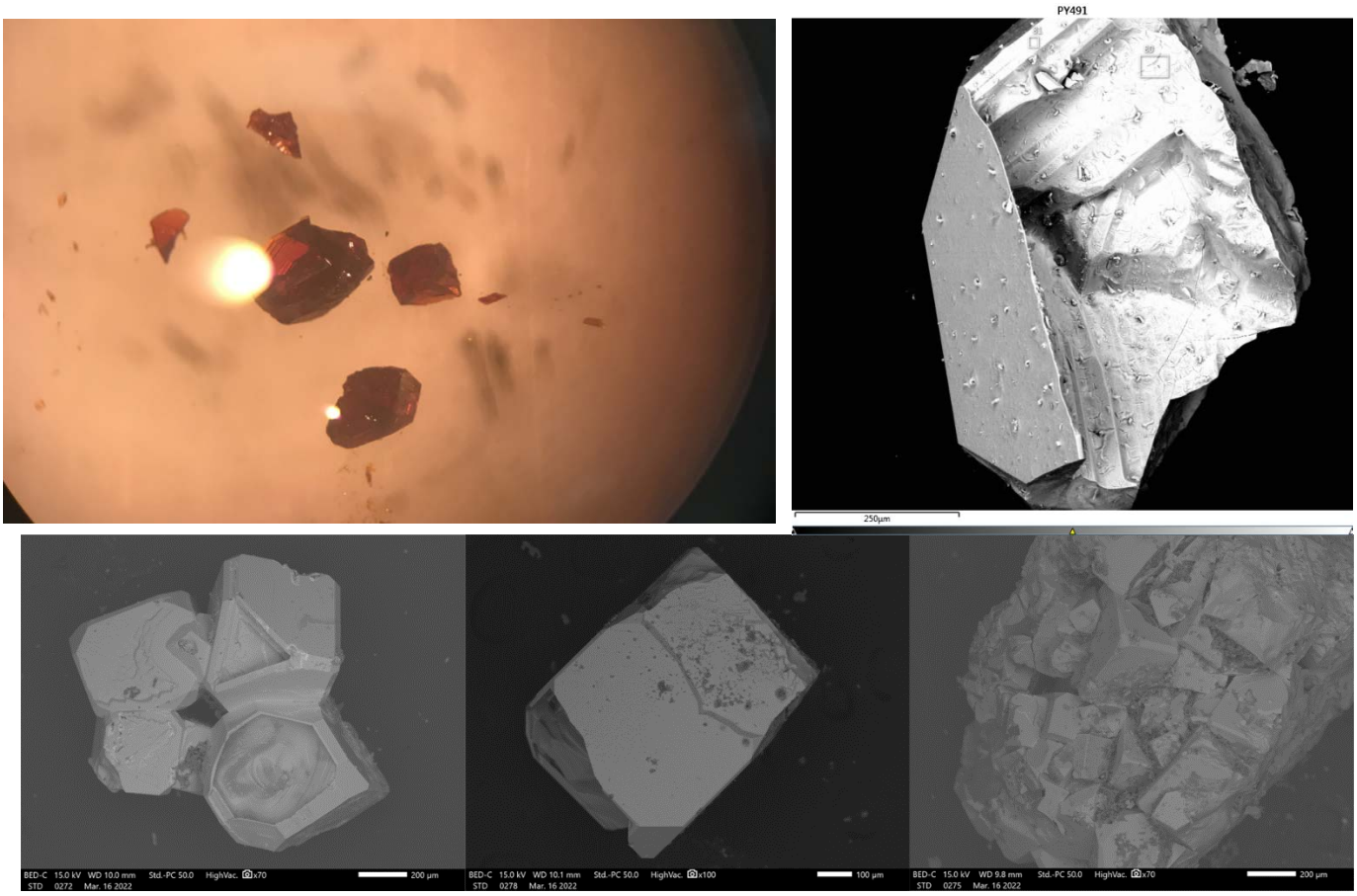

Figure S1. (Top Left) Optical image of $CsBa_6Si_{12}P_{20}Br$ showing their translucent red color and block shape. (Top Right) Scanning electron microscope image of corresponding crystal. (Bottom) Three representative images of $CsBa_6Si_{12}P_{20}I$ crystals grown from CsI flux. Most crystals feature cubelike morphologies but are fused together with other similar crystals.

Table S1. Reaction conditions

	Reaction Conditions for $AAe_6Si_{12}P_{20}X$ compounds			
Composition	Flux/ Stoichiometric	Temperature Profile	H_2O wash	Result
$RbSr_6Si_{12}P_{20}Br$	RbBr flux	10 h ramp to 900°C, 48 h dwell, cool to 800°C over 72 h, NC*	Y	crystals + phase pure powder
$CsSr_6Si_{12}P_{20}Cl$	CsCl flux	10 h ramp to 900°C,144 h dwell, NC	Y	crystals + powder + amorphous phase
$CsSr_6Si_{12}P_{20}Br$	Stoichiometric	10 h ramp to 850°C, 72 h dwell, NC + grind and repeat	N	phase pure powder
$CsSr_6Si_{12}P_{20}Br$	CsBr flux	10 h ramp to 950°C, 120h dwell, NC	Y	crystals + amorphous phase
$CsSr_6Si_{12}P_{20}I$	Stoichiometric	10 h ramp to 850°C, 72 h dwell, NC + grind and repeat	N	phase pure powder
$NaBa_6Si_{12}P_{20}Cl$	NaCl flux	10 h ramp to 1100°C, 24 h dwell, cool to 500°C over 72 h, NC	Y	crystals + powder with impurities
$NaBa_6Si_{12}P_{20}Cl$	Stoichiometric	10 h ramp to 900°C, 48 h dwell, cool to 800°C over 72 h, NC + grind and repeat	N	phase pure powder
$KBa_6Si_{12}P_{20}Cl$	KCl flux	10 h ramp to 1000°C, 72 h dwell, cool to 700°C over 72 h, NC	Y	crystals + phase pure powder
$RbBa_6Si_{12}P_{20}Cl$	RbCl flux	10 h ramp to 1100°C, 24 h dwell, cool to 500°C over 72 h, NC	Y	crystals + phase pure powder
$RbBa_6Si_{12}P_{20}Br$	RbBr flux	10 h ramp to 1000°C, 72 h dwell, cool to 700°C over 72 h, NC	Y	crystals + phase pure powder
$RbBa_6Si_{12}P_{20}I$	RbI flux	10 h ramp to 1000°C, 72 h dwell, cool to 700°C over 72 h, NC	Y	crystals + powder with impurities
$CsBa_6Si_{12}P_{20}Cl$	CsCl flux	10 h ramp to 900°C, 144 h dwell, NC	Y	crystals + phase pure powder after washing
$CsBa_6Si_{12}P_{20}Br$	CsBr flux	10 h ramp to 900°C, 144 h dwell, NC	Y	crystals + powder with impurities
$CsBa_6Si_{12}P_{20}I$	Stoichiometric	10 h ramp to 1000°C, 72 h dwell, NC + grind and repeat	N	phase pure powder
$CsBa_6Si_{12}P_{20}I$	CsI flux	10 h ramp to 950°C, 120h dwell, NC	Y	crystals + amorphous phase

*NC = natural cooling of furnace (i.e. furnace was turned off and allowed to cool to room temperature)

Figure S2. Selected powder X-ray diffraction patterns compared to the calculated pattern determined from the single crystal X-ray diffraction experiment.

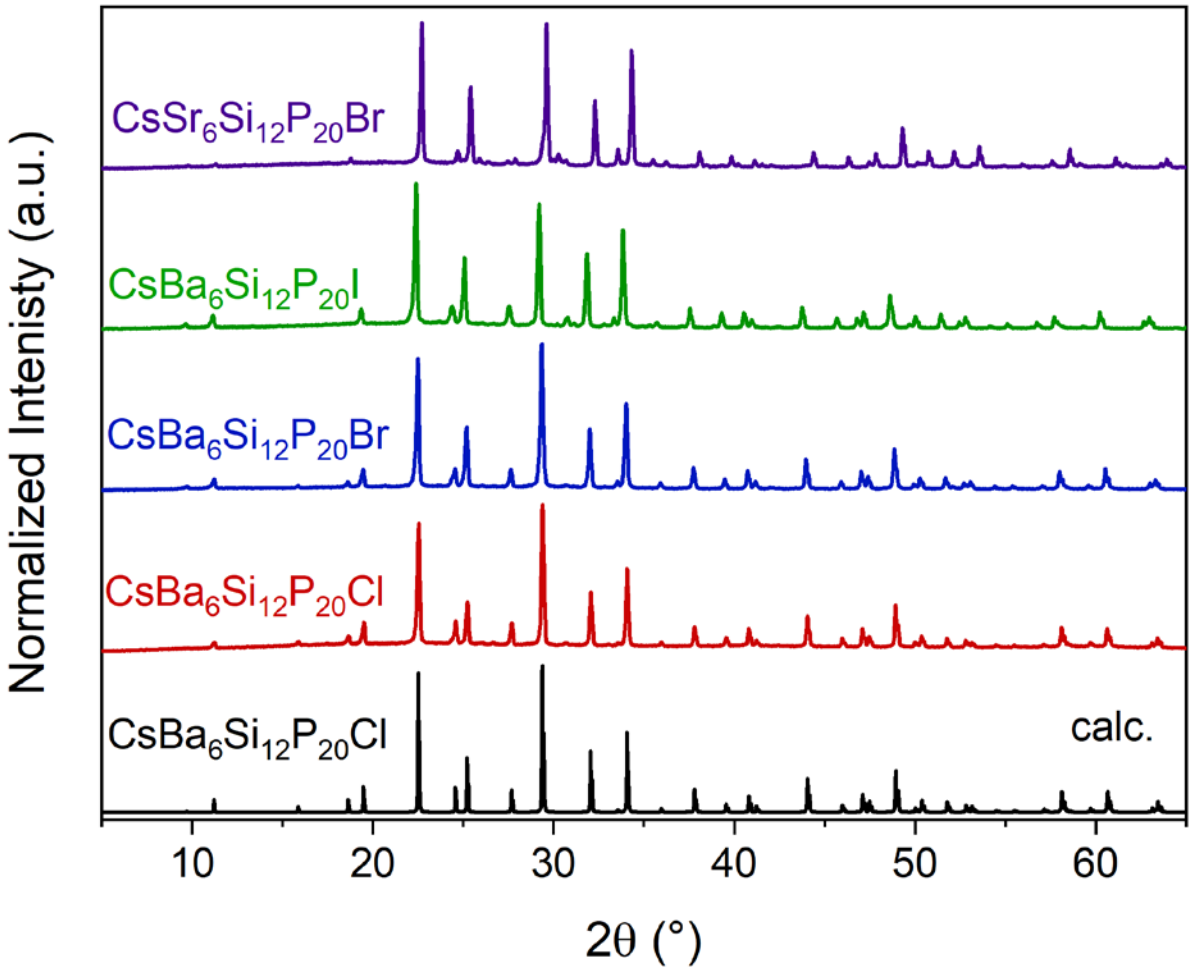

Table S2. Elemental analysis of selected compounds (Energy Dispersive X-ray Spectroscopy)

$CsBa_6Si_{12}P_{20}I$	Cs	Ba	Si	P	I
	2.51	14.81	27.59	52.5	2.58
	2.27	13.16	28.23	53.99	2.35
	2.75	14.78	23.62	56.1	2.75
	2.5	17.09	25.9	51.94	2.57
	2.46	15.3	26.95	52.67	2.62
	2.07	14.68	27.82	53.05	2.38
	2.22	14.87	27.83	52.67	2.41
	2.1	14.17	26.77	54.63	2.33
	1.74	13.13	28.61	54.16	2.36
	2.32	14.93	27.23	53.08	2.44
Average	**2.3**	**15**	**27**	**53**	**2.4**
Standard Deviation	**0.5**	**2**	**1**	**1**	**0.2**
Theoretical	**2.7**	**14.9**	**30**	**50**	**2.3**
$CsBa_6Si_{12}P_{20}Cl$	Cs	Ba	Si	P	Cl
	2.39	14.63	32.42	48.03	2.53
	2.29	14.53	32.67	47.93	2.56
	2.41	15.06	33.01	47	2.53
	2.33	14	32.97	48.14	2.56
	2.3	15.21	33.06	47	2.43
	2.59	16.91	32.3	45.65	2.55
Average	**2.3**	**15.0**	**32.7**	**47.3**	**2.52**
Standard Deviation	**0.1**	**0.9**	**0.3**	**0.9**	**0.04**
Theoretical	**2.5**	**15.0**	**30**	**50**	**2.5**
$CsSr_6Si_{12}P_{20}Br$	Cs	Sr	Si	P	Br
	1.73	14.24	28.74	51.96	3.34
	2.31	14.97	27.83	51.58	3.3
	2.34	14.94	27.5	52.16	3.07
	2.81	16.06	29.13	48.71	3.29
	3.02	16.79	30.67	46.2	3.31
	2.49	14.86	28.51	51.12	3.02
	2.41	15.03	28.15	51.31	3.11
Average	**2.4**	**15.3**	**28.6**	**50.4**	**3.2**
Standard Deviation	**0.4**	**0.8**	**1.0**	**2.0**	**0.1**
Theoretical	**2.5**	**15**	**30**	**50**	**2.5**

Table S3. Crystallographic data and parameters from SXRD experiment.

	$CsBa_6Si_{12}P_{20}I$	$CsBa_6Si_{12}P_{20}Br$	$CsBa_6Si_{12}P_{20}Cl$	$RbBa_6Si_{12}P_{20}I$	$RbBa_6Si_{12}P_{20}Br$	$RbBa_6Si_{12}P_{20}Cl$
Refined Composition	$Cs_{1.0625}Ba_{5.9375}Si_{12}P_{20}I_{0.9375}$	$CsBa_6Si_{12}P_{20}Br$	$CsBa_6Si_{12}P_{20}Cl$	$Rb_{1.1}Ba_{5.9}Si_{12}P_{20}I_{0.9}$	$RbBa_6Si_{12}P_{20}Br$	$RbBa_6Si_{12}P_{20}Cl$
EDS Composition	$Cs_{0.92}Ba_6Si_{11}P_{21}I_{0.96}$	_	$Cs_{0.94}Ba_6Si_{13}P_{19}Cl_1$	_	_	_
CSD Deposition #	2168162	2168172	2168165	2168167	2168171	2168169
Temperature (K)	100					
Radiation (Å)	0.71073					
Crystal System	Cubic					
Space Group	$Fm\bar{3}m$ (No. 225)					
a (Å)	15.8615(6)	15.8173(3)	15.7803(7)	15.8551(5)	15.8031(6)	15.757(3)
Volume (Å^3)	3990.6(5)	3957.3(3)	3929.6(5)	3985.7(4)	3946.6(4)	3912(2)
Z	4					
Data/parameters	419/24	436/23	434/17	435/25	434/18	434/17
Density (g·cm3)	3.396	3.346	3.294	3.321	3.275	3.228
μ (mm^{-1})	8.673	8.976	8.09	8.997	9.316	8.445
R_{int}	0.035	0.025	0.041	0.036	0.041	0.027
GooF	1.189	1.339	1.198	1.258	1.132	1.383
R_1	0.011	0.013	0.013	0.012	0.012	0.011
R_1 [all data]	0.014	0.014	0.015	0.014	0.014	0.012
wR_2 [all data]	0.023	0.032	0.024	0.027	0.023	0.024
Diff. peaks [e·Å^3]	0.44/-0.66	0.46/-1.77	0.44/-0.67	0.50/-0.67	0.63/-1.07	0.37/-0.67

Table S3 continue. Crystallographic data and parameters from SXRD experiment.

	$KBa_6Si_{12}P_{20}Cl$	$NaBa_6Si_{12}P_{20}Cl$	$CsSr_6Si_{12}P_{20}Br$	$CsSr_6Si_{12}P_{20}Cl$	$RbSr_6Si_{12}P_{20}Br$
Refined Composition	$KBa_6Si_{12}P_{20}Cl$	$NaBa_6Si_{12}P_{20}Cl$	$CsSr_6Si_{12}P_{20}Br$	$CsSr_6Si_{12}P_{20}Cl$	$RbSr_6Si_{12}P_{20}Br$
EDS Composition	–	–	$Cs_{1.04}Ba_{6.4}Si_{12}P_{19.6}Br_{1.32}$	–	–
CSD Deposition #	2168168	2168166	2168163	2168164	21681670
Temperature (K)	100				
Radiation (Å)	0.71073				
Crystal System	Cubic				
Space Group	*Fm*$\bar{3}$*m* (No. 225)				
a (Å)	15.7315(6)	15.6717(9)	15.6447(5)	15.6693(7)	15.632(1)
Volume (Å^3)	3893.2(4)	3849.0(7)	3829.1(4)	3847.2(5)	3820(1)
Z	4				
Data/parameters	425/22	424/24	442/18	270/19	271/17
Density (g·cm3)	3.165	3.173	2.94	2.85	2.865
μ (mm^{-1})	7.351	7.338	11.501	10.478	11.855
R_{int}	0.033	0.06	0.05	0.058	0.047
GooF	1.22	1.18	1.12	1.11	1.12
R_1	0.010	0.016	0.016	0.022	0.023
R_1 [all data]	0.010	0.021	0.020	0.026	0.027
wR_2 [all data]	0.022	0.030	0.034	0.054	0.045
Diff. peaks [e·Å^3]	0.49/-0.36	0.48/-0.72	1.13/-2.22	1.13/-1.58	0.78/-1.28

Further details of the crystal structure determination may be obtained from Fachinformationszentrum Karlsruhe, Germany, by quoting the CSD depository numbers given in the Table above.

Table S4. Atomic coordinates as determined by the X-ray diffraction experiment. In many cases, highlighted in yellow, mixing of the alkaline earth metal and alkali metal is observed. The site mixing appears more prominent when the alkali metal is small (Na, K). In the structures containing iodine, highlighted in green, the formation of iodine vacancies requires the adjusted ratio of alkaline earth metal and alkali metal to account for the charge imbalance. The final occupancies of Cs/Ba and Rb/Ba were constrained so that no site had more than 100 +/- 1% occupancy.

Atom	Wyckoff	*x/a*	*y/b*	*z/c*	Occ.	U_{eq} (Å^2)
$Cs_{1.0625}Ba_{5.9375}Si_{12}P_{20}I_{0.9375}$						
Ba1	24*e*	½	0.22165	½	0.970	0.006
Cs11	24*e*	½	0.19504	½	0.030	0.006
Cs1	4*b*	½	½	½	0.867	0.009
Ba11	24*e*	½	½	0.53232	0.020	0.009
I1	4*a*	½	0	½	0.935	0.005
P1	48*i*	½	0.32757	0.67243	1.0	0.005
P2	32*f*	0.33502	0.16498	0.66498	1.0	0.004
Si1	48*g*	0.41251	¼	¾	1.0	0.004
$CsBa_6Si_{12}P_{20}Br$						
Ba1	24*e*	½	0.21708	½	0.972	0.004
Cs11	24*e*	½	0.19880	½	0.028	0.004
Cs1	4*b*	½	½	½	0.815	0.006
Ba11	24*e*	½	½	0.5222	0.028	0.006
Br1	4*a*	½	0	½	1.0	0.007
P1	48*i*	½	0.32812	0.67188	1.0	0.003
P2	32*f*	0.33526	0.16474	0.66474	1.0	0.003
Si1	48*g*	0.41251	¼	¾	1.0	0.002
$CsBa_6Si_{12}P_{20}Cl$						
Ba1	24*e*	½	0.21607	½	1.0	0.004
Cs1	4*b*	½	½	½	1.0	0.007
Cl1	4*a*	½	0	½	1.0	0.007
P1	48*i*	½	0.32832	0.67168	1.0	0.003
P2	32*f*	0.33536	0.16464	0.66464	1.0	0.003
Si1	48*g*	0.4265	¼	¾	1.0	0.002
$Rb_{1.1}Ba_{5.9}Si_{12}P_{20}I_{0.9}$						
Ba1	24*e*	½	0.22096	½	0.941	0.006
Rb11	24*e*	½	0.19289	½	0.074	0.006
Rb1	4*b*	½	½	½	0.66	0.019
Ba11	24*e*	½	½	0.52390	0.042	0.019
I1	4*a*	½	0	½	0.891	0.005
P1	48*i*	½	0.32778	0.67222	1.0	0.004
P2	32*f*	0.33513	0.16487	0.66487	1.0	0.004
Si1	48*g*	0.41208	¼	¾	1.0	0.003

$RbBa_6Si_{12}P_{20}Br$						
Ba1	24*e*	½	0.21790	½	0.985	0.005
Rb11	24*e*	½	0.21790	½	0.019	0.005
Rb1	4*b*	½	½	½	0.888	0.012
Ba11	24*e*	½	0.47464	½	0.015	0.012
Br1	4*a*	½	0	½	1.0	0.006
P1	48*i*	½	0.32823	0.67177	1.0	0.003
P2	32*f*	0.33530	0.16470	0.66470	1.0	0.003
Si1	48*g*	0.41248	¼	¾	1.0	0.003
$RbBa_6Si_{12}P_{20}Cl$						
Ba1	24*e*	½	0.2155	½	0.984	0.004
Rb11	24*e*	½	0.2155	½	0.017	0.004
Rb1	4*b*	½	½	½	0.900	0.012
Ba11	24*e*	½	0.52744	½	0.017	0.004
Cl1	4*a*	½	0	½	1.0	0.007
P1	48*i*	½	0.32856	0.67144	1.0	0.003
P2	32*f*	0.33545	0.16455	0.66455	1.0	0.003
Si1	48*g*	0.41270	¼	¾	1.0	0.002
$KBa_6Si_{12}P_{20}Cl$						
Ba1	24*e*	½	0.24160	½	0.939	0.004
K11	24*e*	½	0.24160	½	0.061	0.004
K1	24*e*	½	0.52409	½	0.105	0.014
Ba11	24*e*	½	0.52409	½	0.062	0.014
Cl1	4*a*	½	0	½	1.0	0.008
P1	48*i*	½	0.32872	0.67128	1.0	0.003
P2	32*f*	0.33561	0.16439	0.66439	1.0	0.003
Si1	48*g*	0.41260	¼	¾	1.0	0.003
$NaBa_6Si_{12}P_{20}Cl$						
Ba1	24*e*	½	0.21161	½	0.839	0.006
Na11	24*e*	½	0.23055	½	0.161	0.006
Na1	24*e*	½	½	0.52571	0.005	0.023
Ba11	24*e*	½	½	0.52571	0.161	0.023
Cl1	4*a*	½	0	½	1.0	0.010
P1	48*i*	½	0.32911	0.67089	1.0	0.005
P2	32*f*	0.33601	0.16399	0.66399	1.0	0.004
Si1	48*g*	0.41232	¼	¾	1.0	0.004
$CsSr_6Si_{12}P_{20}Br$						
Sr1	24*e*	½	0.22618	½	1.0	0.007
Cs1	4*b*	½	½	½	1.0	0.008
Br1	4*a*	½	0	½	1.0	0.017
P1	48*i*	½	0.32918	0.67082	1.0	0.003
P2	32*f*	0.33627	0.16373	0.66373	1.0	0.005
Si1	48*g*	0.41240	¼	¾	1.0	0.003

$CsSr_6Si_{12}P_{20}Cl$						
Sr1	24*e*	½	0.22186	½	0.931	0.009
Sr11	24*e*	½	0.22469	½	0.069	0.009
Cs1	4*b*	½	½	½	1.0	0.007
Cl1	4*a*	½	0	½	1.0	0.067
P1	48*i*	½	0.32758	0.67242	1.0	0.004
P2	32*f*	0.33612	0.16389	0.66389	1.0	0.008
Si1	48*g*	0.41237	¼	¾	1.0	0.003
$RbSr_6Si_{12}P_{20}Br$						
Sr1	24*e*	½	0.22590	½	1.0	0.008
Rb1	4*b*	½	½	½	1.0	0.017
Br1	4*a*	½	0	½	1.0	0.012
P1	48*i*	½	0.32939	0.67061	1.0	0.004
P2	32*f*	0.33645	0.16355	0.66355	1.0	0.005
Si1	48*g*	0.41235	¼	¾	1.0	0.003

Table S5. Atomic distances in $CsBa_6Si_{12}P_{20}Cl$ as determined from SXRD.

Atom 1	Atom 2	Distance (Å)
Si1	P1	2.2259(6)
Si1	P2	2.2620(4)
Cs1	P1	3.8314(6)
Ba1	P1	3.2368(2)
Ba1	P2	3.7627(5)
Ba1	Cl1	3.4097(2)
Ba1	Cs1	4.4804(3)
Cs1	P2	6.4425(6)

Figure S3: Alkali Metal occupancy of 4*b* and 24*e* sites. At the center of the cuboctahedron (light blue) lies the 4*b* site. The 4*b* site occupancy is plotted on the left y-axis. As the 4*b* site occupancy decreases, the disordered A11 24*e* site occupancy (plotted on the right y-axis) increases. The A11 24*e* site lies in the truncated octahedron (purple).

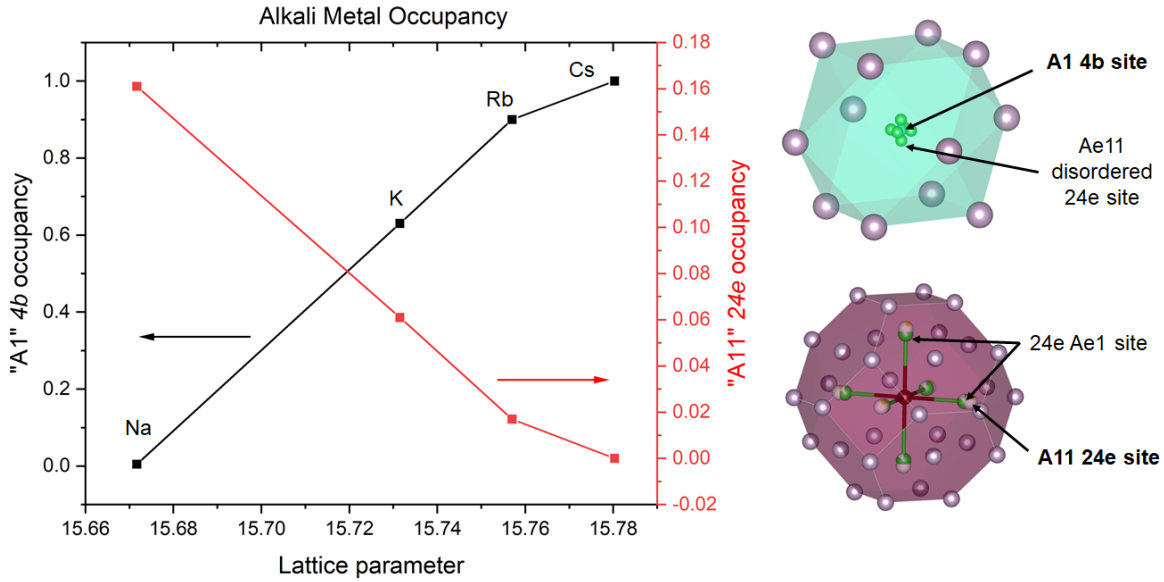

Table S6: Experimental NMR parameters

Figure	Expt.	B_0 (T)	MAS (kHz)	Recycle Delay (s)	# of scans	t_1 TD Points	Δt_1 (μs)	Expt. time (h)
2A	^{31}P Spin echo	9.4	10	500	8	-	-	1.1
2A	^{31}P Spin Echo	9.4	8	500	8	-	-	1.1
2B	^{29}Si Spin Echo	9.4	10	7200	8	-	-	32.0
2C	^{133}Cs Spin Echo	9.4	10	2000	2	-	-	1.1
2C	^{133}Cs 90^{o} SP	14.1	10	400	8	-	-	0.9
2D[a]	^{31}P {^{133}Cs} D-HMQC	9.4	10	50	8	88	100	9.7
S4	^{35}Cl Spin Echo	9.4	10	2	16384	-	-	9.1
S7[b]	^{133}Cs EXSY	9.4	10	30	8	80	100	5.3

[a]Recorded with either 0.8 or 4.0 ms of heteronuclear dipolar recoupling. [b]Recorded with either a 1 μs or 0.5 s Z spin-diffusion period and a sample temperature of either 38 or 58 ^{O}C.

Table S7. ^{31}P analytical simulation NMR parameters[a]

Phosphorus Coordination	δ_{iso} (ppm)	δ (ppm)[b]	η	Population (%)	Total Population (%)
2	–54.0	64.8	0.00	27.8	59
2	–55.8	81.5	0.29	15.6	
2	–63.8	79.9	0.09	15.4	
3	–171.1	55.2	0.10	3.0	41
3	–174.3	41.1	0.09	9.0	
3	–175.5	42.7	0.08	8.5	
3	–178.5	24.6	0.12	13.6	
3	–182.1	44.3	0.10	4.2	
3	–185.9	51.7	0.03	3.1	

[a]8 kHz MAS frequency. [b]Reduced anisotropy.

Table S8. ^{29}Si analytical simulation NMR parameters

δ_{iso} (ppm)	Population
–15.5	42.8%
–10.7	57.2%

Table S9. ^{133}Cs analytical simulation NMR parameters. The simulation suggest that Cs is equally as likely to occupy either the Cs or Ba site.

δ_{iso} (ppm)	C_Q (kHz)[a]	9.4 T Population (%)[b]	14.1 T Population (%)[c]
212.4	600	39	30
206.0	500	61	70

[a]η = 0 for all sites. [b]Quantitative NMR spectrum. [c]NMR spectrum was ran with a non-quantitative recycle delay.

Figure S4: 1D ^{35}Cl spin echo solid-state NMR spectrum recorded at B_0 = 9.4 T. Two groups of ^{35}Cl NMR signals are indicated by the asterisks.

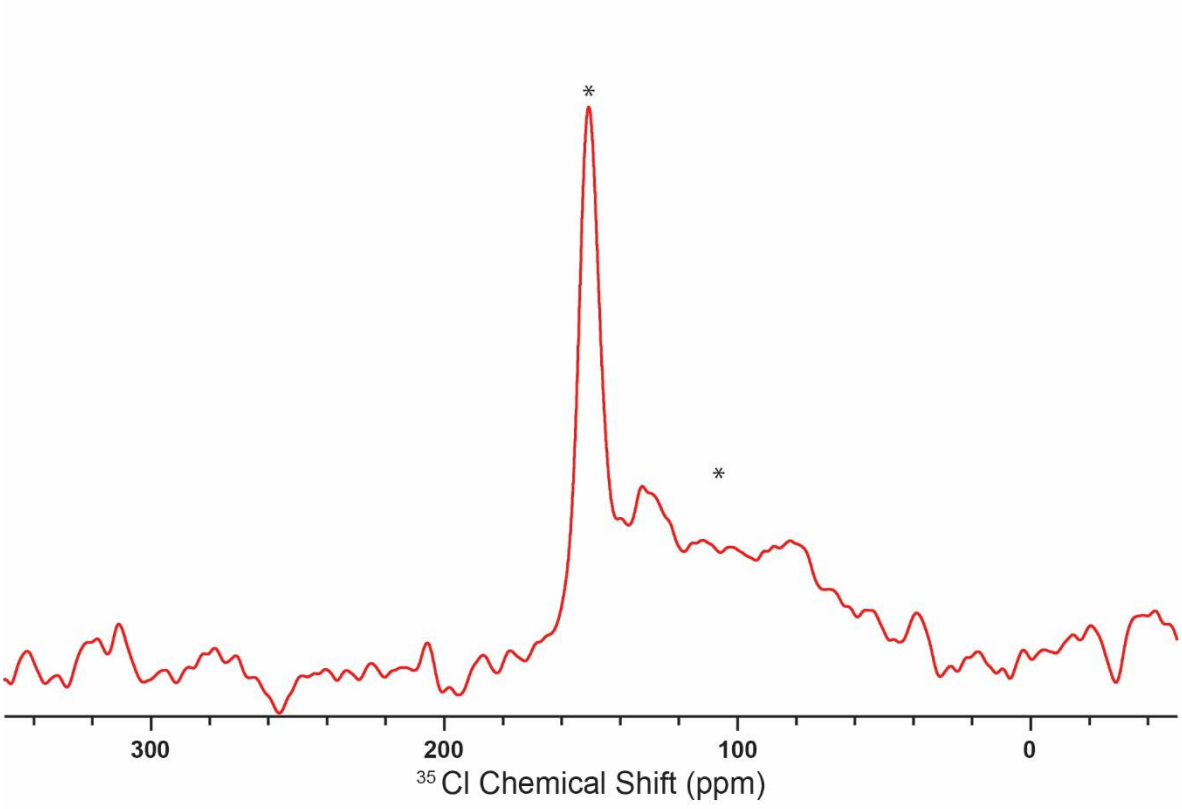

Figure S5: Zoom-in of the 2D $^{31}P\{^{133}Cs\}$ D-HMQC NMR spectrum recorded with 0.8 ms of dipolar recoupling shown in Figure 2D of the main text. The purple and pink circles overlaid on the 2D contour lines indicate the two unique ^{31}P NMR signals.

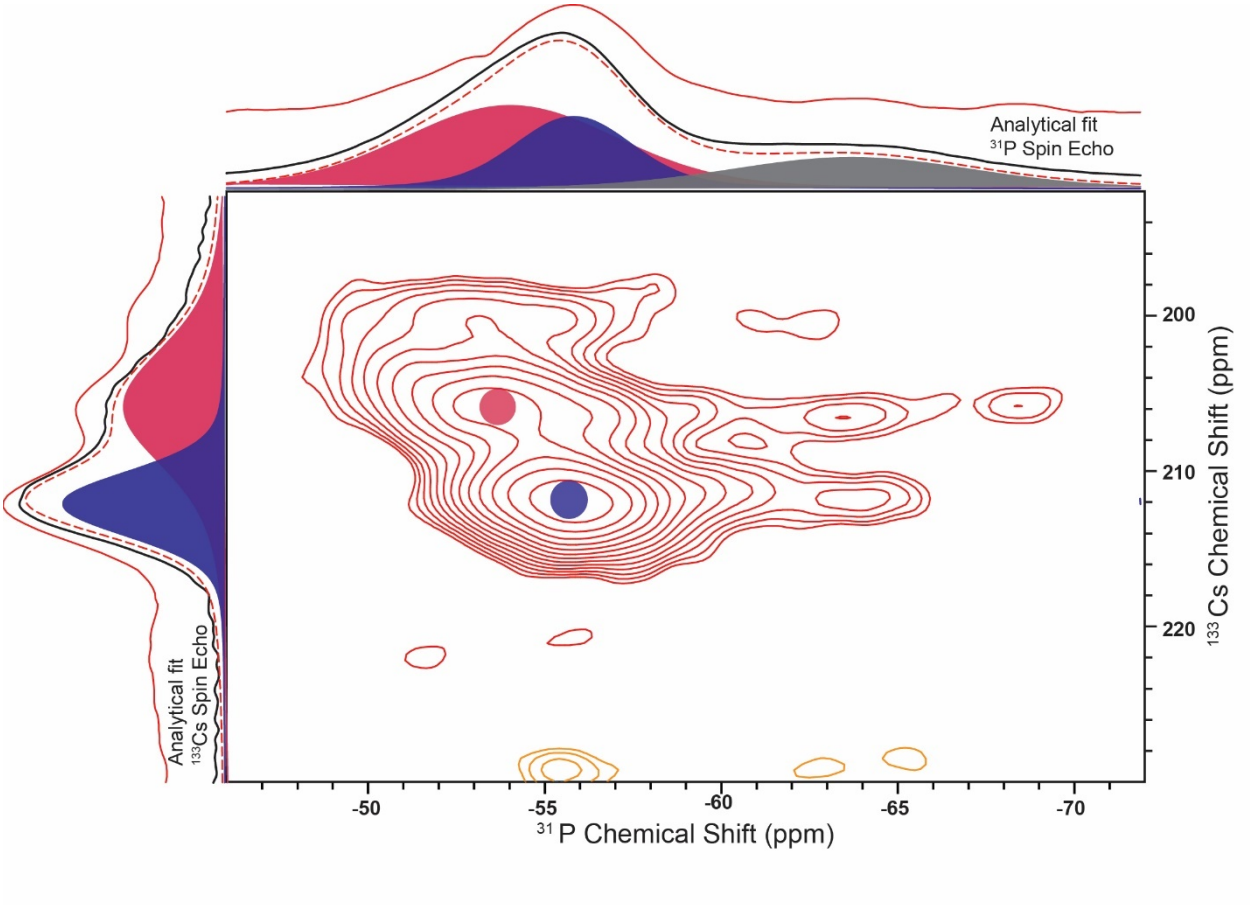

Figure S6: ^{29}Si NMR signal intensity as a function of recycle delay for the ^{29}Si NMR signals centered at *ca.* (blue) –10 and (orange) –15 ppm. Experimental data points are shown as circles and analytical fits of the ^{29}Si T_1 are shown as solid lines (mono-exponential).

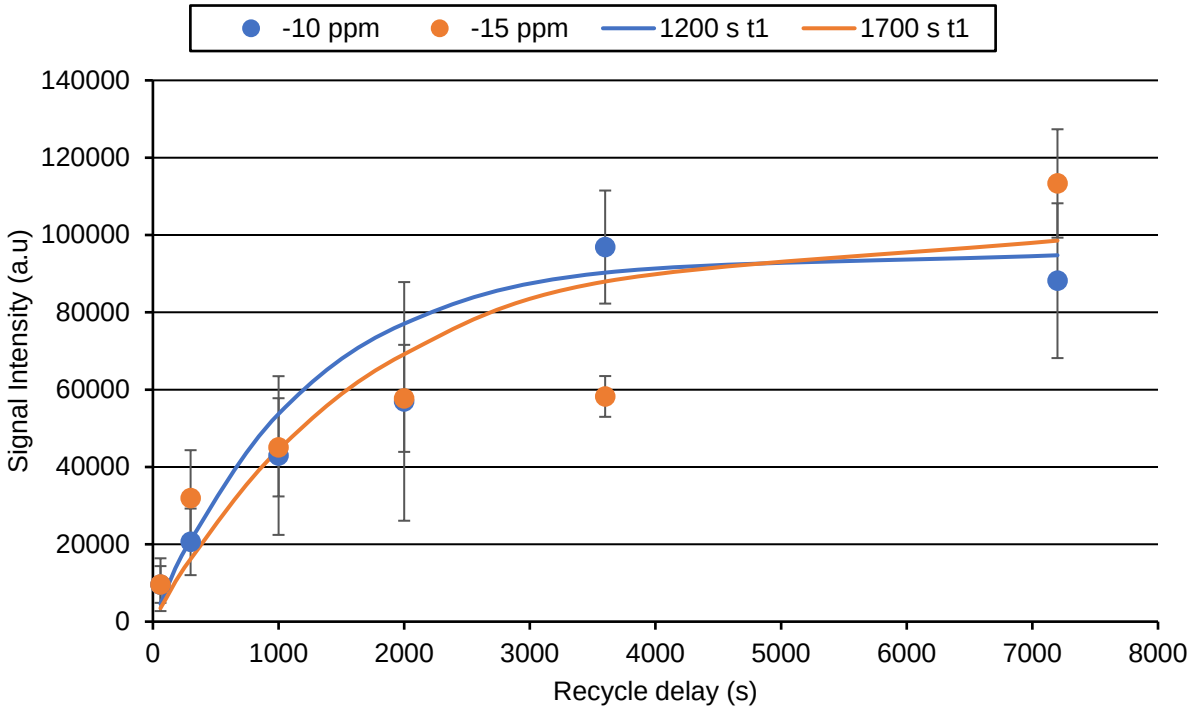

Figure S7: 2D ^{133}Cs EXSY NMR spectra recorded with a (blue) 1 μs or (red) 0.5 s Z spin-diffusion period (τ_{SD}) and a sample temperature of *ca.* (A) 38°C or (B) 58°C. No correlations between the two ^{133}Cs sites is observed, suggesting these sites are relatively far from one another and no Cs site hopping occurs at these temperature ranges.

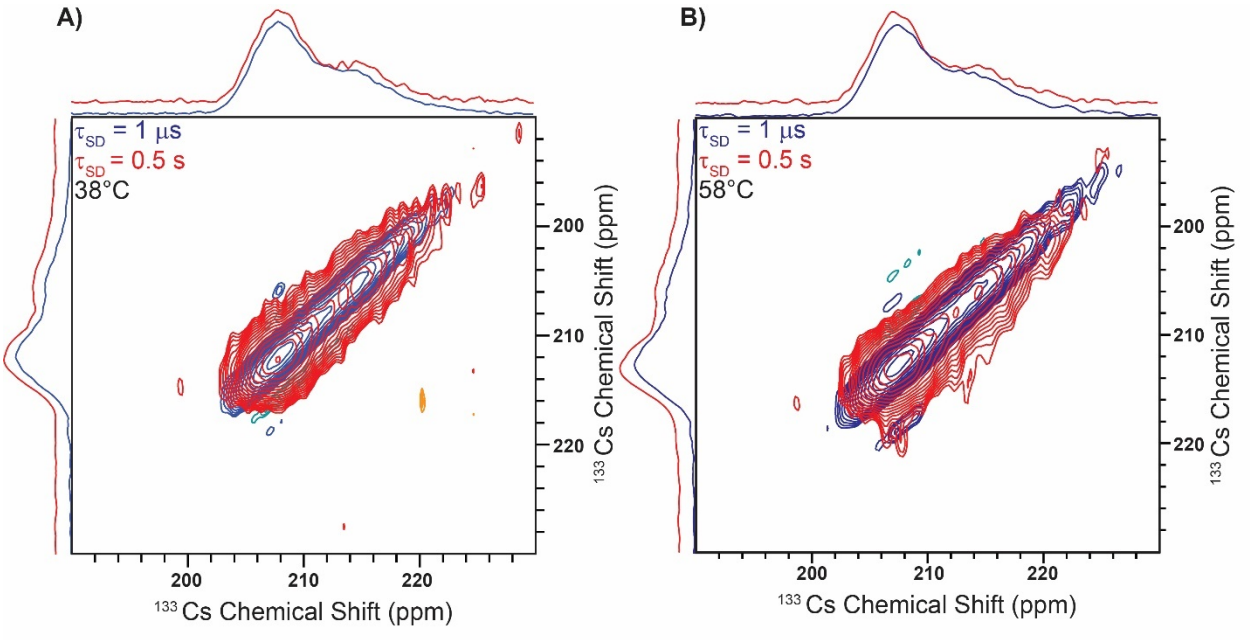

Figure S8. Differential scanning calorimetry results for $CsBa_6Si_{12}P_{20}Br$.

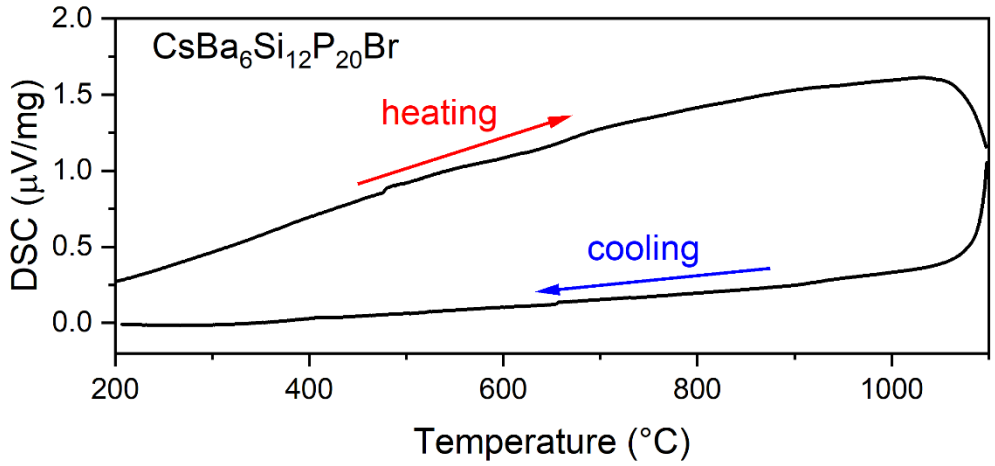

Figure S9. Tauc plots from UV-vis diffuse reflectance spectroscopy measurements.

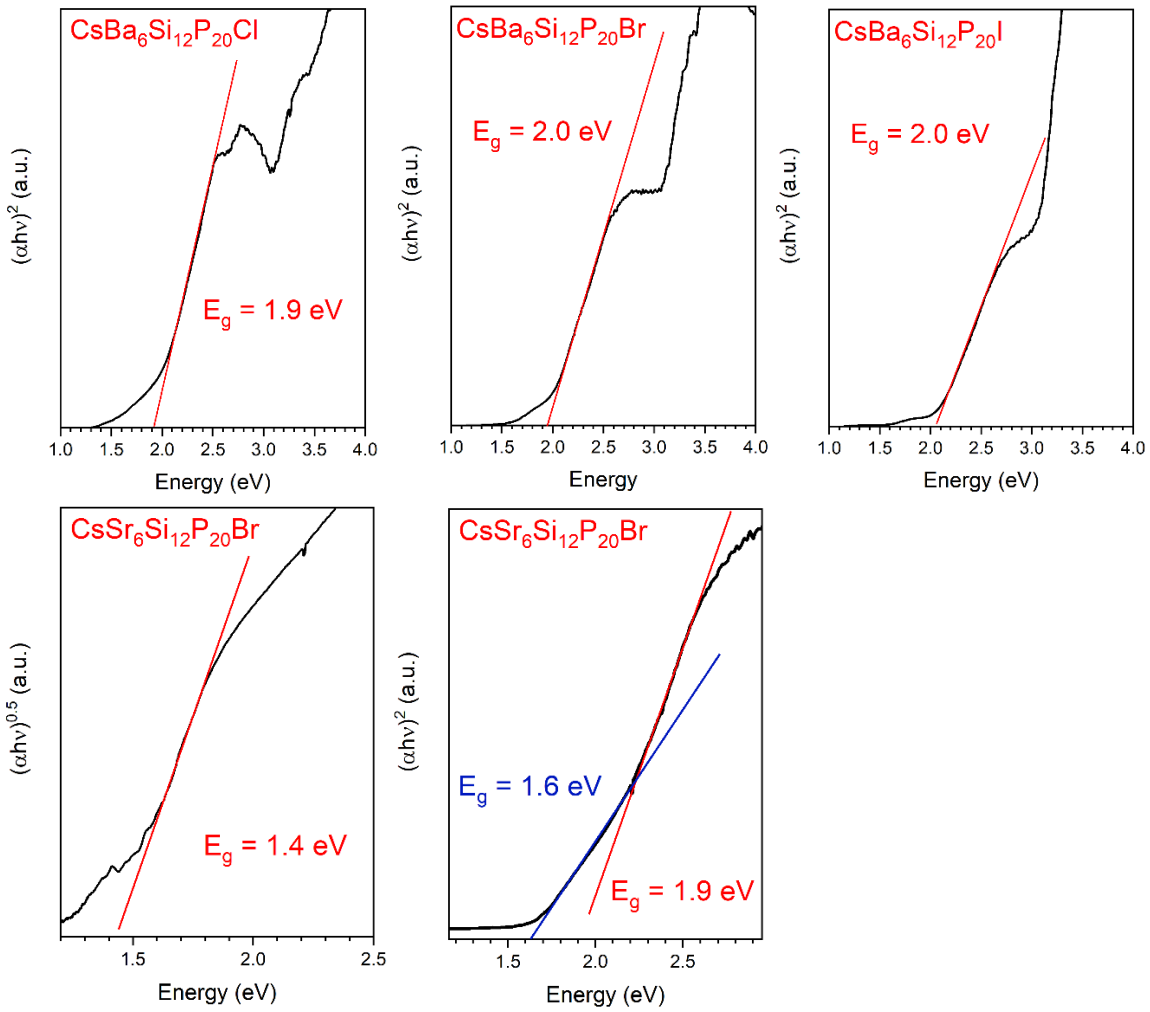

Figure S10. Band structures of $CsBa_6Si_{12}P_{20}Cl$, $CsBa_6Si_{12}P_{20}Br$, and $CsSr_6Si_{12}P_{20}Br$